Applied Surface Science 436 (2018) 791–802

Contents lists available at ScienceDirect

Applied Surface Science

journal homepage: www.elsevier.com/locate/apsusc

Full Length Article

Hydrophobic and hydrophilic nanosheet catalysts with high catalytic activity and recycling stability through control of the outermost ligand

Younji Ko [1], Donghee Kim [1], Cheong Hoon Kwon, Jinhan Cho *

Department of Chemical & Biological Engineering, Korea University, 145 Anam-ro, Seongbuk-gu, Seoul, 02841, Republic of Korea

ARTICLE INFO

Article history:
Received 16 August 2017
Received in revised form
23 November 2017
Accepted 6 December 2017
Available online 13 December 2017

Keywords:
Hydrophobic/hydrophilic graphene oxide nanosheet
Palladium nanoparticle
Ligand replacement reaction
TMB oxidation
Suzuki–Miyaura coupling reaction

ABSTRACT

In this study, we introduce hydrophobic and hydrophilic graphene oxide nanosheet (GON) catalysts prepared by consecutive ligand replacement of hydrophobically stabilized magnetic and catalytic nanoparticles (NPs); it exhibits high catalytic activity, fast magnetic response, and good dispersion in both nonpolar and aqueous media, allowing high loading amount of magnetic and catalytic NPs onto GON sheets. More specifically, these GON catalysts showed a high product yield of 66–99% and notable recyclability (93% of the initial product yield after 10 reaction cycles) in a Suzuki–Miyaura reaction in nonpolar media, outperforming the performance of the conventional hydrophilic GON catalysts. Additional coating of a hydrophilic layer onto GON catalysts also showed the notable performance (product yield ~99%) in catalytic reactions performed in aqueous media. Given that ligand-controlled catalytic NPs adsorbed onto 2D nanosheets can be used as hydrophobic and hydrophilic stabilizers as well as catalysts, our approach can provide a tool for developing and designing 2D-nanosheet catalysts with high performance in nonpolar and polar media.

1. Introduction

Metal nanoparticle (NP)-based catalysts have been widely used in a number of chemical reaction-related processes such as photocatalysts or the synthesis of fine chemicals (including intermediates or pharmaceutical products), and electrochemical applications owing to their high surface-to-volume ratio and unusual active sites for better catalytic performance [1–6]. Important parameters for the preparation of high-performance NP catalysts are uniform and stable immobilization of well-defined active NPs on solid substrates with a large surface area and high dispersion of the formed catalyst-supported substrates in desired reaction media. More specifically, because the catalytic reaction of noble metals such as palladium (Pd) in the heterogeneous or semi-heterogeneous catalysis for carbon–carbon (C—C) coupling reactions occurs almost entirely on the particle surface [7–10], a high dispersion of catalytic NPs in the reaction media is required to enhance the catalytic activity. However, NPs without appropriate ligands easily aggregate in aqueous or organic reaction media, reducing their catalytic activity [11,12].

As an alternative, a number of approaches have been developed for the preparation of catalytic NPs with stable immobilization on various solid supports, including carbon-based materials [13–25]. In particular, graphene oxide nanosheets (GONs) have drawn considerable attention owing to their enormous surface area (2630 $m^2 g^{-1}$) [23–25]. For example, most hydrophilic Pd NP-supported GONs (prepared by the direct reduction of Pd ions or by electrostatic assembly) exhibit high catalytic activity in hydrophilic reaction media (*i.e.,* water and/or water/alcohol mixture) but not in nonpolar media because of their poor dispersion stability and stacking phenomenon [26,27]. Pd NP-supported GONs showed high catalytic activity (product yield ~99%) for Suzuki–Miyaura reaction in water or methanol/water mixture [28,29]. However, the product yield in nonpolar media was in the range ~5–69%. Although highly dispersible GON sheets can be prepared in nonpolar media by introducing organic moieties with long alkyl chains onto the surface of the GON sheet [30,31], the resulting GON sheets had no interaction with the surface of the hydrophilic or hydrophobic catalytic NPs. Thus, the 2D-sheet catalysts, such as GON sheet/catalytic nanocomposites have mainly been prepared *via* metal ion reduction or electrostatic assembly that can induce uniform dispersion in only aqueous or water/alcohol mixture media rather than organic media. In this case, the packing density (or loading amount) of catalytic NPs on hydrophilic GONs is limited to the level where the NPs decorate the surface. As a result, a substantial portion of the large surface area remains inactive or bare. Therefore, interface control of catalytic NPs and GONs is strongly required for the development

* Corresponding author.
E-mail address: jinhan71@korea.ac.kr (J. Cho).
[1] These authors contributed equally to this work.

https://doi.org/10.1016/j.apsusc.2017.12.037
0169-4332/

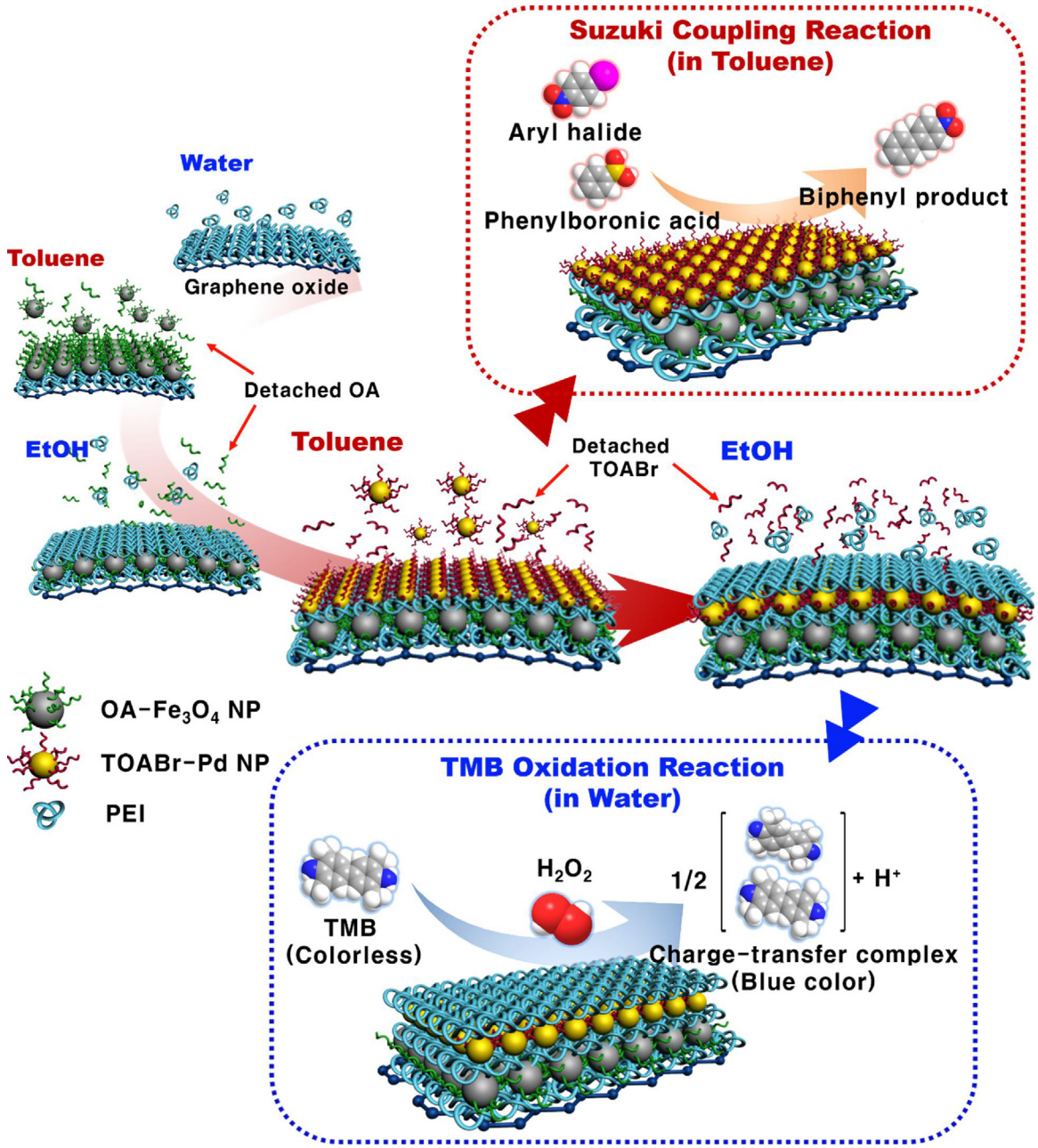

Scheme 1. Schematic for the preparation of hydrophobic and hydrophilic GON catalysts containing OA-Fe_3O_4 NPs and TOABr-Pd NPs.

of high-performance 2D-nanosheet catalysts that are highly active, stable and dispersible in both nonpolar and polar media.

Herein, we introduce for the first time hydrophobic and hydrophilic GON catalysts with high catalytic activity, good reusability, and high dispersion in both nonpolar and aqueous reaction media. Particularly, we highlight that these hydrophobic and hydrophilic 2D-nanosheet catalysts can be prepared by an aid of the outermost ligand-controllable NPs. Another remarkable features are that our approach can maximize the effectiveness of 2D-nanosheets with large specific surface area, and furthermore significantly enhance the recyclability as a result of densely packed magnetic NPs as well as covalent bonding between 2D-nanosheet and catalytic NPs. As model systems for demonstrating these uniquenesses, Suzuki–Miyaura reaction in polar/nonpolar media and 3,3′,5,5′-tetramethylbenzidine (TMB) oxidation in aqueous media were performed using hydrophobic and hydrophilic GON catalysts. First, the GON catalysts composed of poly(ethylene imine) (PEI), tetra(octylammonium bromide)-stabilized Pd (TOABr-Pd NPs) [32], and oleic acid-stabilized Fe_3O_4 NPs (OA-Fe_3O_4 NPs) [33] were prepared using ligand-replacement reaction assembly (Scheme). When the hydrophobic TOABr-Pd NPs were deposited onto GONs, the yield of various aryl iodides and phenylboronic acids in toluene using these hydrophobic catalysts increased up to 99%. Their catalytic activity was 2.8 and 12 times higher than those of conventional GON catalysts and other multi-wall carbon nanotube (MWCNT)-type catalysts in nonpolar media, respectively. In addition, when the outermost ligand on the Pd NPs was changed from hydrophobic TOABr to hydrophilic PEI, the catalyst again exhibited high catalytic performance (product yield ~99%) for the Suzuki–Miyaura coupling reactions in water or alcohol media and for the oxidation of 3,3′,5,5′-tetramethylbenzidine (TMB) in aqueous media. Furthermore, the GON catalysts displayed

fast separation from the reaction mixture by virtue of their densely packed Fe_3O_4 NPs, which imparted high recycling stability. The importance of our approach is the ability to impart hydrophobic/hydrophilic and high catalytic properties to GONs through ligand control and large surface area of GONs. Given that this strategy can be easily applied to other functional metal or metal oxide NPs, our approach can provide a tool for developing novel functional nanocomposites as well as high-performance recyclable catalysts for use in various reaction media.

2. Experimental

2.1. Materials

All the materials used in our study were purchased from Sigma-Aldrich and Alfa Aesar and used without additional purification.

2.2. Preparations

2.2.1. Synthesis of graphene oxide nanosheets

Graphene oxide nanosheets (GONs) were synthesized from natural graphite by the Hummers method [34]. First, preoxidized graphite powder (0.5 g) and $NaNO_3$ (0.5 g) were placed in concentrated H_2SO_4 (23 mL) at 0 °C. $KMnO_4$ (3 g) was added to the reaction mixture, while the temperature was maintained below 20 °C. The mixture was then stirred at 37 °C for 1 h followed by adding hot deionized (DI) water (40 mL) at 90 °C. After 30 min, 34.5% H_2O_2 (3 mL) and 100 mL of DI water were added to quench the reaction. Next, the graphite oxide was suspended in DI water to give a brown dispersion, which was dialyzed to completely remove salts and acids. The resulting purified graphite oxide powder was collected by centrifugation and dried under vacuum. The obtained graphite oxide was dispersed in water *via* sonication to affording graphene oxide.

2.2.2. Synthesis of Carboxylic acid-fuctionalized MWCNTs (MWCNT-COOH)

MWCNT-COOH were prepared following the literature [35]. Pristine MWCNTs were oxidized by a mixture of H_2SO_4/HNO_3 at 70 °C for 3 h to prepare MWCNT-COOH. The resulting suspensions were then dialyzed for 3 days to remove all the salts and acids, and the purified MWCNT-COOH powder was collected by filtration and dried under vacuum. The MWCNT-COOH was redispersed in ethanol *via* sonication.

2.2.3. Synthesis of OA-Fe_3O_4 NPs

OA-Fe_3O_4 NPs were prepared following the literature [36]. For the synthesis of OA-stabilized Fe_3O_4 NPs, $Fe(acac)_3$ (2 mmol), 1,2-hexadecanediol (10 mmol), oleic acid (5 mmol), oleylamine (6 mmol), and benzyl ether (20 mL) were mixed and magnetically stirred under a flow of nitrogen. The reaction mixture was heated to 200 °C for 2 h and then refluxed (~300 °C) for 1 h under a blanket of nitrogen. After heating, the black-colored mixture was allowed to cool to room temperature. Ethanol (40 mL) was added to the mixture under ambient conditions, inducing precipitation of a black material that was subsequently separated *via* centrifugation. The black product was dissolved in a toluene solution containing OA (0.05 mL) and oleylamine (0.05 mL). Undispersed residue was removed *via* centrifugation (6000 rpm, 10 min), affording. OA-Fe_3O_4 NPs were synthesized with a diameter of 7.33-nm and characterized by Fourier transform infrared spectroscopy (FTIR) in the attenuated total reflection mode (ATR) (Figs. S1 and S2 in the Supplementary data).

2.2.4. Synthesis of anionic-Fe_3O_4 NPs

For the preparation of anionic Fe_3O_4 NP dispersions, the OA-Fe_3O_4 NPs (10 mg mL^{-1}) were transferred from toluene to aqueous media using water-dispersible polyhedral silsesquioxane (PSS) hydrate octakis(tetramethylammonium) (10 mmol) [37]. The resulting octakis-Fe_3O_4 NP solution was isolated using a separatory funnel.

2.2.5. Synthesis of TOABr-Pd NPs

TOABr-Pd NPs were prepared as reported previously [32]. For the synthesis of TOABr-stabilized Pd NPs with a diameter of 2.61-nm, an aqueous solution of 30 mM aqueous K_2PdCl_4 (30 mL) was first added to 25 mM TOABr in toluene (80 mL). Transfer of the K_2PdCl_4 from the aqueous phase to the toluene phase was observed within 1 min. A solution of 0.4 M $NaBH_4$ (25 mL) was added to the reaction mixture. After 30 min, the separated aqueous phase was removed and the toluene solution containing the reduced TOABr-Pd NPs was subsequently washed sequentially with 0.1 M H_2SO_4, 0.1 M NaOH, and H_2O. TOABr-Pd NPs were synthesized with a diameter of 2.61-nm and characterized by ATR-FTIR (Figs. S1 and S2 in the Supplementary data).

2.2.6. Synthesis of cationic-Pd NPs

Cationic Pd NPs were prepared as reported previously [32]. For the synthesis of cationic Pd NPs, an aqueous solution of 0.1 M 4-dimethylaminopyridine (DMAP) (80 mL) was added to the as-prepared TOABr-Pd NP toluene solution (80 mL). In this case, the Pd NPs were directly phase-transferred from toluene to the aqueous phase within 3 h and the toluene phase was subsequently removed. The resulting Pd NPs were stabilized by cationic DMAP ligands in water (*i.e.,* DMAP-Pd NPs).

2.2.7. Synthesis of OA-TiO_2 NPs

For the preparation of OA-stabilized TiO_2 NPs [38], tert-butylamine (0.1 mL) was dissolved in DI water (10mL), and 0.15 g of titanium(IV) n-propoxide (0.5 mmol) and 1.0 mL of OA were dissolved in 10 mL of toluene. The solution was transferred to an autoclave, sealed, and maintained at 180 °C for 12 h, followed by washing with methanol. The OA-TiO_2 NPs were isolated by centrifugation and dispersed in toluene.

2.2.8. Synthesis of OA-Ag NPs

For the preparation of OA-stabilized Ag NPs [39], silver trifluoroacetate (0.4 g), OA (3.5 mL) and isoamyl ether (30 mL) were mixed in a 250 mL three-neck flask under argon. The mixture was heated at 160 °C for 30 min, and cooled to room temperature. The purification process was performed four times using excess polar solvent (ethanol) and centrifugation. The precipitated OA-Ag NPs were dispersed in toluene.

2.2.9. Synthesis of OA-Pt NPs

For the preparation of OA-stabilized Pt NPs [40], $Pt(acac)_2$ (0.2 g), OA (2 mL), oleylamine (2 mL), and 1-octadecene (20 mL) were mixed in a 250 mL three-neck flask under argon. The flask was heated to 120 °C and maintained at this temperature for 30 min. A solution of $Fe(CO)_5$ in hexane (0.1 mL, prepared by adding $Fe(CO)_5$ in 1 mL of hexane) was rapidly injected into the flask. The mixture was then heated at 200 °C for 1 h. After the completion of the reaction, excess isopropanol was added to the reaction mixture and centrifuged. This process was performed five times using excess isopropanol and centrifugation. The precipitated OA-Pt NPs were dispersed in toluene.

2.2.10. GON/NP nanosheets using ligand-replacement reaction

For consecutive ligand-replacement adsorption of PEI and hydrophobic NPs onto GONs, 1 mL of a concentrated disper-

sion (0.1 wt%) of negatively charged GONs was centrifuged at 12,000 rpm for 20 min. After centrifugation, the supernatant was removed and a PEI solution of 5 mg mL^{-1} was added to the GON sediment, followed by ultrasonication for 30 min. Excess PEI was removed *via* two centrifugation (12,000 rpm, 20 min)/wash cycles. In this case, the deposition of PEI onto GONs were confirmed by ATR-FTIR and Raman spectroscopy (Fig. S3).

To deposit hydrophobic NPs onto the PEI-coated GON, a hydrophobic NP solution (*i.e.,* TOABr-Pd or OA-Fe_3O_4 NPs in toluene) with a concentration of 10 mg mL^{-1} was again added to the PEI-coated GONs. The adsorption and washing cycles of the hydrophobic NPs were exactly identical to those used for PEI.

2.2.11. GON/NP nanosheets using electrostatic adsorption

For the electrostatic adsorption assembly of the GON/NP nanosheets (charged polyelectrolyte/oppositely charged NP), 1 mL of a concentrated dispersion (0.1 wt%) of the negatively charged GONs was centrifuged at 12,000 rpm for 20 min. After centrifugation, the supernatant was removed and a PEI solution of 5 mg mL^{-1} was added to the GON sediment, followed by ultrasonication. Excess PEI was removed *via* two centrifugation (12,000 rpm, 20 min)/wash cycles. For the electrostatic adsorption of anionic (PSS hydrate octakis(tetramethylammonium) stabilized)-Fe_3O_4 NPs [37] onto the cationic PEI-coated GONs (*i.e.,* GON/PEI/Octakis-Fe_3O_4 NP), an aqueous Octakis-Fe_3O_4 NP solution with a concentration of 10 mg mL^{-1} was added to the PEI-coated GONs. To deposit cationic (4-dimethylaminopyridine (DMAP) stabilized)-Pd NPs [32] onto the anionic poly(styrene sulfonate) (PSS)/PEI-coated GONs (*i.e.,* GON/PEI/PSS/DMAP-Pd NP), an anionic PSS solution with a concentration of 10 mg mL^{-1} was added to the cationic PEI-coated GONs. After adsorption of anionic PSS, a cationic DMAP-Pd NP solution with a concentration of 10 mg mL^{-1} was added to the PSS/PEI-coated GONs. In addtion, to prepare GON/PEI/Octakis-Fe_3O_4 NP/PEI/PSS/DMAP-Pd NP nanosheets, all the adsorption and washing cycles of PEI, Octakis-Fe_3O_4 NP, PSS, and DMAP-Pd NP were identical to the adsorption procedures previously described.

2.2.12. GON/NP nanosheets using direct metal ion reduction

For the direct metal ion reduction assembly of Pd NPs onto PEI-coated GON (*i.e.,*GON/PEI/OA-Fe_3O_4 NP/PEI), the nanosheets were prepared as previously reported by other research groups, with a slight modification [41]. A tetrachloropalladate solution (H_2PdCl_4) was prepared using $PdCl_2$ and HCl in DI water. This solution was stirred at 60 °C and then cooled to room temperature. H_2PdCl_4 (10 mM, 20 mM) and $NaBH_4$ (1 M) solutions were added dropwise to a stirring suspension of GONs. Excess $NaBH_4$ was removed *via* two centrifugation (12,000 rpm, 20 min)/wash cycles with water and ethanol.

2.2.13. Preparation of NP-supported MWCNTs

For the ligand-replacement assembly of PEI and hydrophobic NPs onto MWCNTs, 1 mL of a concentrated dispersion (0.1 wt%) of negatively charged MWCNTs was centrifuged at 12,000 rpm for 20 min. After centrifugation, the supernatant was removed. The adsorption processes of PEI and hydrophobic NPs onto MWCNTs were exactly identical to those performed for GONs.

2.3. Characterizations

The crystallinity and structure of the NPs (*i.e.*, TOABr-Pd and OA-Fe_3O_4 NPs), catalytic NP-coated GONs and catalytic NP-coated MWCNTs were investigated by high-resolution transmission electron microscopy (HR-TEM, model: Tecnai G2, F30ST).

Vibrational spectra were measured by Fourier transform infrared spectroscopy (FTIR, model: iS10 FT-IR, Thermo Fisher) in the attenuated total reflection (ATR) mode and advance grazing angle specular reflectance (AGA) mode. The sample chamber was purged with nitrogen gas for 2 h to eliminate water and CO_2 prior to the FTIR measurements. ATR-FTIR and AGA-FTIR spectra for the PEI/hydrophobic NP/PEI film deposited onto the Au-coated substrate were obtained from 256 scans with an incident angle of 80°. The acquired raw data were plotted after baseline correction, and the spectra were smoothed using spectrum-analysis software (OMNIC, Nicolet).

Raman spectra were measured using a Horiba Jobin Yvon LabRam Aramis with an Ar-ion laser beam at an exciting radiation wavelength of 514.5 nm.

The zeta potentials of GON/PEI/OA-Fe_3O_4 NP/PEI/TOABr-Pd NP/PEI nanosheets were measured using an electrophoretic light-scattering spectrophotometer (Zeta-potential & Particle size Analyzer ELSZ, OTSUKA ELECTRONICS CO. LTD.) at 633 nm, with a scattering angle of 165°. All the experiments were conducted at 20 °C.

The amounts of Pd embedded within catalytic GON/PEI/OA-Fe_3O_4 NP/PEI/TOABr-Pd NP nanosheets and the Pd leached into the supernatant solution (*i.e.*, the reaction solution following removal of catalytic nanosheets after the cycling test) were determined by inductively coupled plasma mass spectrometry (ICP-MS, model Elan DRC II, PerkinElmer).

The magnetic properties of nanosheets (*i.e.,* GON/PEI/Octakis-Fe_3O_4 NP and GON/PEI/OA-Fe_3O_4 NP) were characterized by a superconducting quantum interference device-vibrating sample magnetometer (SQUID-VSM, model MPMS-XL).

The crystal structures of the inorganic NPs (*i.e.*, OA-Fe_3O_4 NPs and TOABr-Pd NPs) that were coated onto the GONs were characterized by X-ray diffraction (XRD, model D/MAX-2500V/PC, Rigaku). Data collection was performed in the 2θ range 5–90° using Cu Kα radiation (λ = 1.54 Å).

The products of Suzuki–Miyaura coupling reaction were characterized by nuclear magnetic resonance spectroscopy (NMR, model 500 MHz, Varian NMR Systems). Detailed information regarding the ^{1}H NMR (500 MHz) and ^{13}C NMR (125 MHz) NMR data are provided in the Supplementary data. The NMR spectra were referenced to TMS as an internal standard and are reported as follows: chemical shift multiplicity (s = singlet, d = doublet, t = triplet, m = multiplet), coupling constant in Hz, and integration.

2.3.1. Suzuki–Miyaura reaction

Pd-containing catalytic GONs (3 mg) were added to 3 mL of solvent containing aryl halide (1 mmol), phenylboronic acid (2 mmol), base (4 mmol), and tetrabutylammonium bromide (TBAB) (2 mmol). The reaction mixture was magnetically stirred at boiling temperature under Ar. The reaction mixture was cooled to room temperature, and the crude products were purified by column chromatography on 230–400 mesh silica gel using ethyl acetate and hexane (1:10 v/v) as the eluant. The isolated compounds were analyzed by ^{1}H NMR (500 MHz) and ^{13}C NMR (125 MHz), with the chemical shifts reported relative to residual $CDCl_3$ solvent peaks (^{1}H NMR: 0 ppm, ^{13}C NMR: 77.01 ppm) and tetramethylsilane (TMS) as an internal standard. Detailed information for the samples is given in the Supplementary data.

2.3.2. TMB oxidation reaction

Oxidation of 3,3′,5,5′-tetramethylbenzidine (TMB) was performed in a 0.1 M NaOAc buffer solution (50 mL, pH 4.0) with 0.3 mM TMB and 100 mM H_2O_2 at 40 °C. The total amount of GON/PEI/OA-Fe_3O_4 NP/PEI/TOABr-Pd NP/PEI nanosheets used for the TMB oxidation was fixed at 0.05 mg. At given time intervals, 3 mL aliquots were collected from the solution. After the experiment, the catalytic GONs were removed by centrifugation or using a hand-held magnet, and the degree of TMB oxidation was

analyzed by measuring the absorbance peak intensity of TMB at 653 nm *via* UV–vis spectroscopy (Lambda 35 UV–vis spectrometer, PerkinElmer).

2.3.3. Recycling tests

The reusability of the magnetically responsive GON catalysts (*i.e.,* GON/PEI/OA-Fe_3O_4 NP/PEI/TOABr-Pd NP and GON/PEI/OA-Fe_3O_4 NP/PEI/TOABr-Pd NP/PEI nanosheets) was examined in both nonpolar media (corresponding to the Suzuki–Miyaura coupling reaction by Pd NPs) and aqueous media (corresponding to TMB oxidation by Pd NPs and Fe_3O_4 NPs). The catalytic activities were measured after the addition of the recyclable catalytic GONs in each cycle; the nanocomposites were then magnetically separated by a hand-held magnet. The separated GON catalysts were rinsed several times and used in the next cycle. Recycling measurements for the Suzuki–Miyaura reaction and TMB oxidation were carried out in a manner identical to the aforementioned procedure.

3. Results and discussion

For the preparation of hydrophobic and hydrophilic GON catalysts, we first synthesized magnetically retrievable 7.3-nm OA-Fe_3O_4 NPs and catalytically active 2.6-nm TOABr-Pd NPs (see the Supplementary data, Fig. S1). The carboxylic acid-functionalized OA ligands (for OA-Fe_3O_4 NPs) and ammonium-functionalized TOABr ligands (for TOABr-Pd NPs) on the surface of the NPs were easily replaced by the amine groups of PEI during assembly because of the higher affinity of the amine groups with the surface of the metal (or metal oxide) NPs. The ligand-replacement reaction was confirmed using Fourier-transform infrared spectroscopy

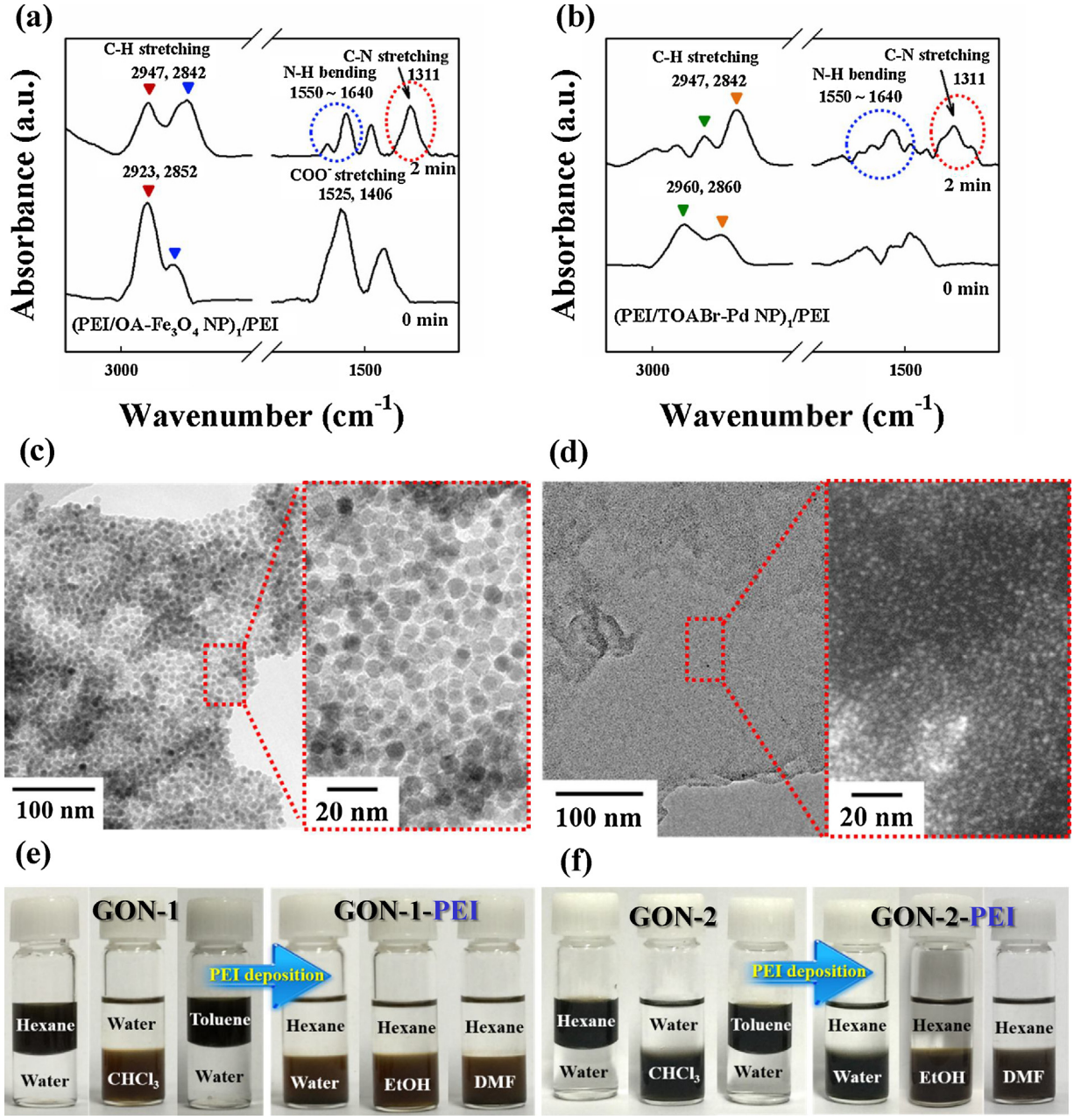

Fig. 1. (a) AGA-FTIR spectra of Au-coated substrate/(PEI/OA-Fe_3O_4 NP)$_1$/outermost PEI and (b) Au-coated substrate/(PEI/TOABr-Pd NP)$_1$/outermost PEI; spectra were collected before and after the deposition of the outermost PEI layer. TEM images of (c) GON-1 and (d) GON-2. (e) Photographic images of GON-1 in nonpolar media and GON-1-PEI in hydrophilic media. Photographic images of (f) GON-2 in nonpolar media and GON-2-PEI in hydrophilic media.

(FTIR) (Figs. 1a, b, and S2 in the Supplementary data). In the case of Au-coated substrate/(PEI/OA-Fe_3O_4 NP)$_1$, noticeable absorption peaks derived from C-N stretching (at 1311 cm^{-1}) of PEI and COO^- stretching (at 1525–1406 cm^{-1}) of OA ligands bound to the surface of Fe_3O_4 NPs were observed as shown in Fig. 1a. However, when the PEI layer was further adsorbed onto the OA-Fe_3O_4 NP-coated film (*i.e.*, Au-coated substrate/(PEI/OA-Fe_3O_4 NP)$_1$/outermost PEI), the absorption peak intensity of the COO^- stretching mode in the range 1525–1406 cm^{-1} significantly decreased, and on the other hand the C—N stretching peak intensity increased. Similarly,

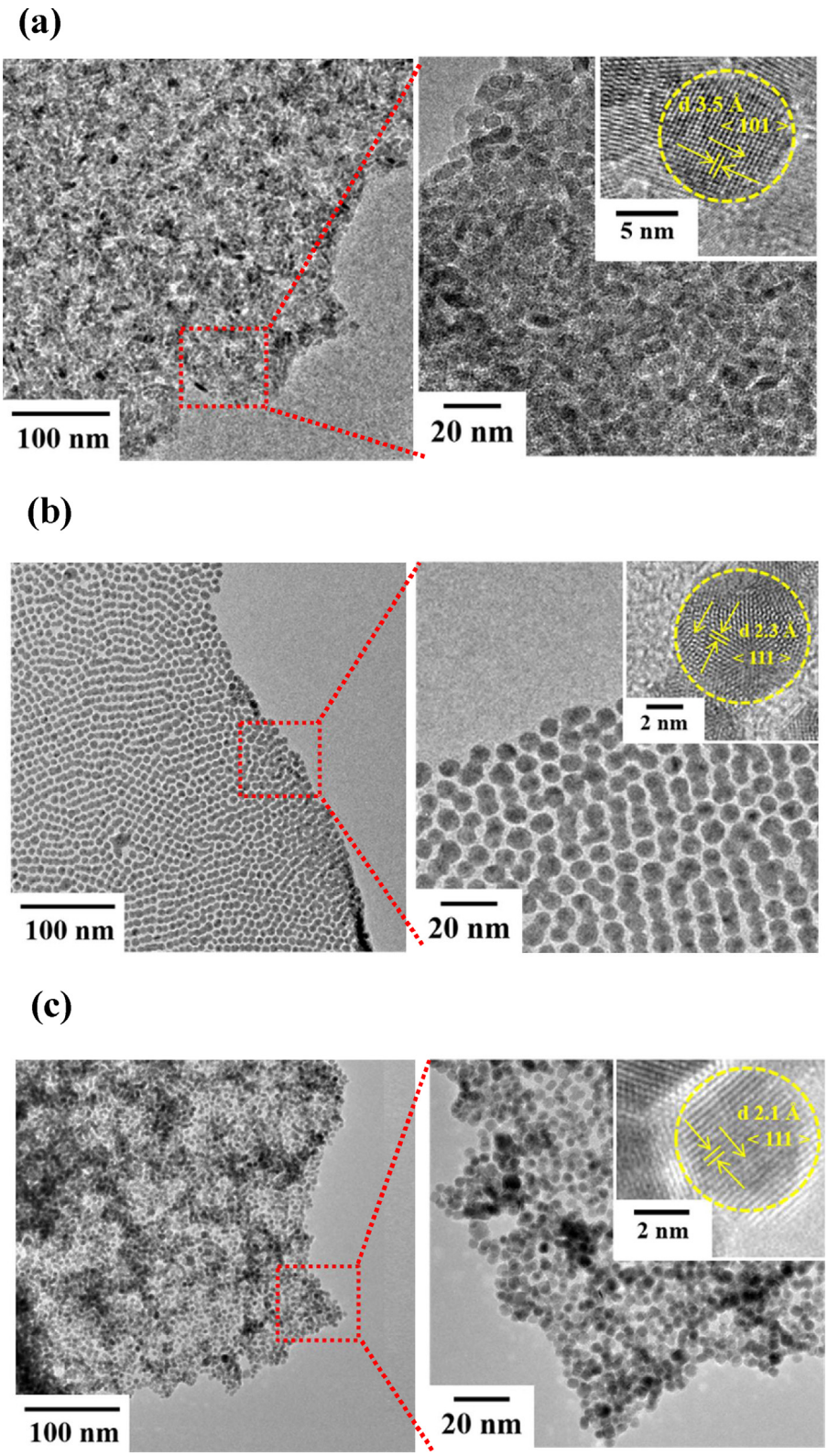

Fig. 2. TEM images of (a) GON/PEI/OA-TiO_2 NPs, (b) GON/PEI/OA-Ag NPs, and (c) GON/PEI/OA-Pt NPs. TEM images show the spacing of the lattice fringes of the TiO_2 NPs (3.5 Å), the Ag NPs (2.3 Å) and the Pt NPs (2.1 Å), which correspond to the TiO_2 (101), Ag (111) and Pt (111) crystalline planes, respectively.

when PEI as an outermost layer was deposited onto the Au-coated substrate/(PEI/TOABr-Pd NP)$_1$, the intensity of the C—H stretching peak (at 2960 cm^{-1}) originating from the long aliphatic chains of TOABr decreased notably, whereas the intensity of the N—H bending peaks in the range 1550–1560 cm^{-1} and C—N stretching peaks at 1311 cm^{-1} originating from the amine groups of PEI increased (Fig. 1b). In addition, the hydrophobic NPs were densely but uniformly adsorbed onto the PEI-coated GONs because there was no electrostatic repulsion among the neighboring NPs in organic media (Fig. 1c and d). More specifically, after the deposition of OA-Fe_3O_4 or TOABr-Pd NPs, the formed GONs were converted into hydrophobic GON hybrids (*i.e.,* GON/PEI/OA-Fe_3O_4 NP, designated as GON-1, and GON/PEI/TOABr-Pd NP, designated as GON-2) that could be dispersed in nonpolar media (Fig. 1e and f). Although it was reported that pristine GONs have amphiphilic properties due to the presence of the hydrophilic edges (COOH groups) and hydrophobic basal plane [42], these GONs in our system were easily aggreagted in organic media (Fig. S4).

However, when the outermost ligand on the NPs was changed from OA (or TOABr) to PEI, the GON hybrids (*i.e.,* GON/PEI/OA-Fe_3O_4 NP/PEI (GON-1-PEI); GON/PEI/TOABr-Pd NP/PEI (GON-2-PEI)) were well-dispersed in alcohol and aqueous media. The neutral amine groups of the outermost PEI ligands bound to the NP-coated GONs in alcohol were converted into protonated amine groups in water (the pK_a of PEI∼10), generating highly dispersible GON hybrids with a zeta potential value of 42.7 ± 1.1 mV in water. Similar phenomena were applied to other hydrophobic NPs, including OA-TiO_2 [43], OA-Ag [44], or OA-Pt NPs [40] (Figs. 2 and S5). As a result, the replacement of the ligands bound to the outermost NPs plays a significant role in preparing highly dispersible GON catalysts in organic and aqueous media by preventing strong π–π stacking interactions between the adjacent GONs.

In contrast, it should be noted that traditional preparation methods for catalytic NP-coated GONs do not effectively exploit the advantages of 2D-nanosheet supports with large surface area. For example, the deposition of catalytic NPs onto PEI-coated GONs by the electrostatic adsorption or the direct metal ion reduction method [41] in aqueous solution limits the packing density of the NPs to only decoration level because the electrostatic repulsion between NPs with the same charge or is restricted to the use of dilute metal ion concentrations, respectively (Fig. 3). In particular, the metal ion reduction method in aqueous media has much difficulty in controlling the loading amount and size of catalytic NPs on the solid support. Although the use of a metal precursor solution with relatively high concentration can increase the loading amount of catalytic NPs onto GONs, it also accelerates the formation of aggregated NPs, exhibiting poor activity. Furthermore, these GON catalysts can not be dispersed in organic media.

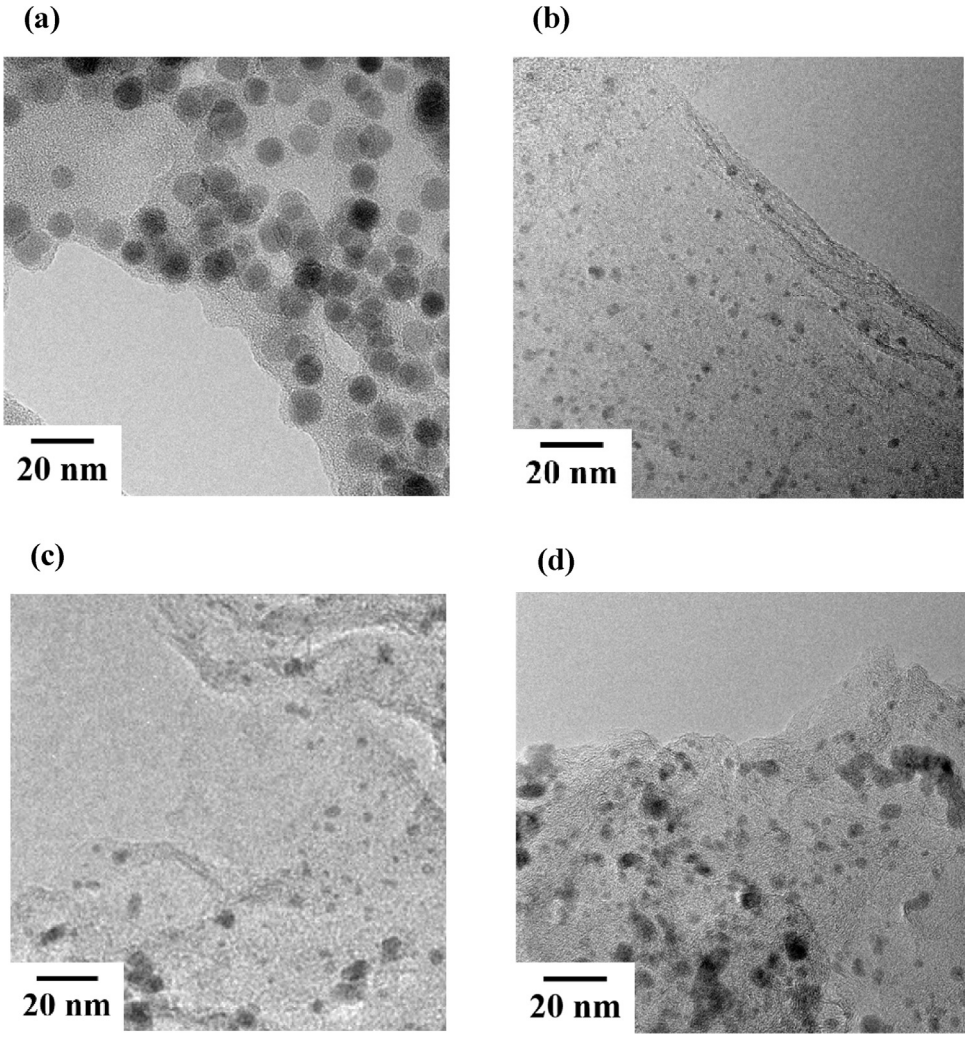

Fig. 3. TEM images of the electrostatic adsorption-assembled nanosheets (a) anionic Fe_3O_4 NP-coated GONs (*i.e.,* GON/PEI/Octakis-Fe_3O_4 NP) and (b) cationic Pd NP-coated GONs (*i.e.,* GON/PEI/PSS/DMAP-Pd NP), and Pd NPs on PEI-coated GONs prepared by direct metal ion reduction in aqueous solutions containing (c) 10 mM and (d) 20 mM H_2PdCl_4.

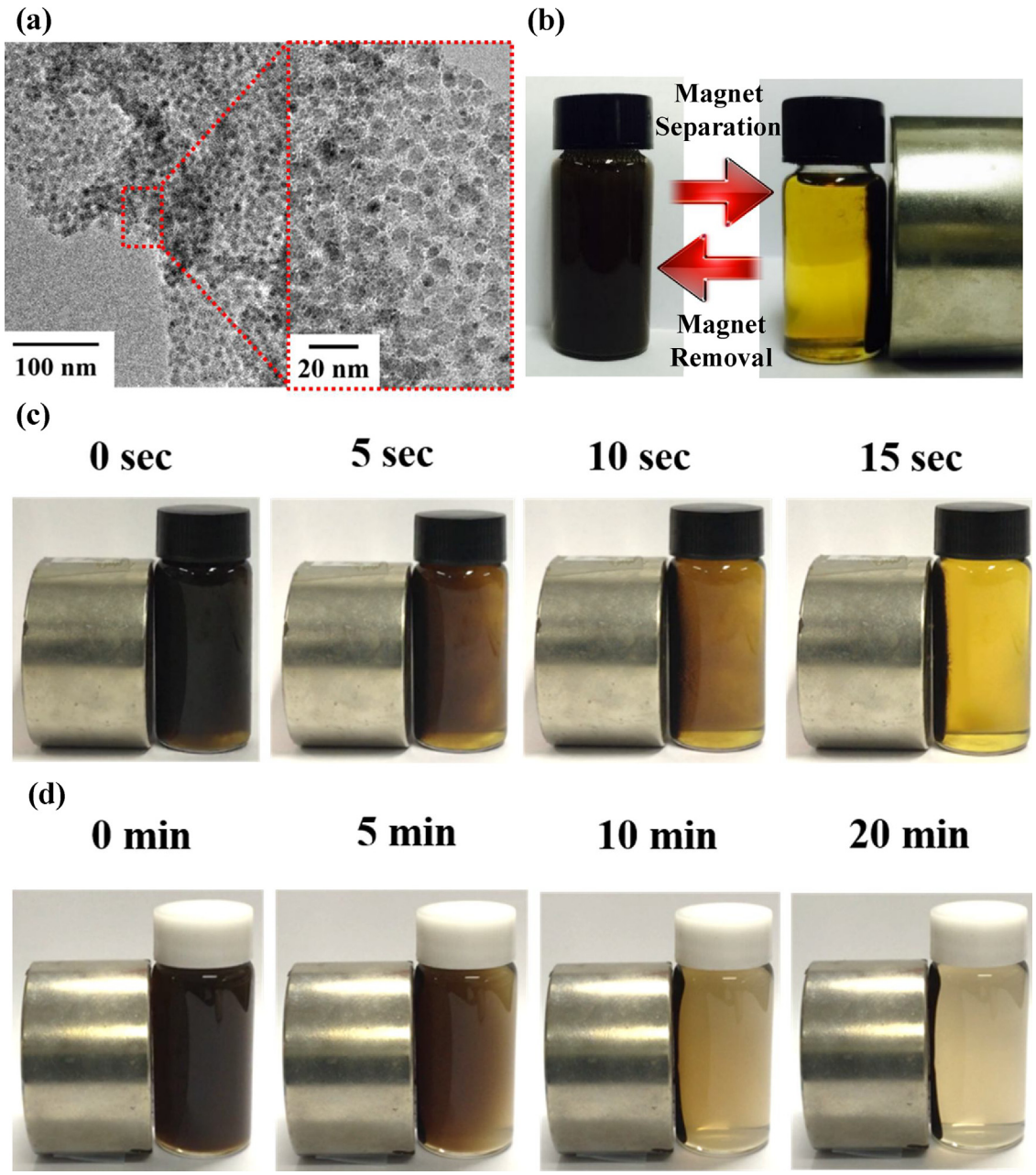

Fig. 4. (a) TEM images of GON-3 (*i.e.*, GON/PEI/OA-Fe_3O_4 NP/PEI/TOABr-Pd NP). (b) Photographic images demonstrating the magnetic responsive properties of GON-3 in toluene. Time-dependent photographic images of (c) GON-3 (*i.e.*, GON/PEI/OA-Fe_3O_4 NP/PEI/TOABr-Pd NP) in toluene and (d) electrostatic adsorption nanosheets (*i.e.*, GON/PEI/Octakis-Fe_3O_4 NP/ PEI/PSS/DMAP-Pd NP) with magnetic responsive properties in water.

To overcome these problems, magnetically retrievable and hydrophobic/hydrophilic GON catalysts composed of OA-Fe_3O_4 and TOABr-Pd NPs were prepared by consecutive ligand-replacement reactions. First, the high packing density, uniform composition, and typical crystalline state of the NPs (*i.e.*, Fe_3O_4 and Pd NPs) within the GON hybrids (*i.e.*, GON/PEI/OA-Fe_3O_4/PEI/TOABr-Pd, shortly GON-3) were confirmed by HR-TEM, energy-dispersive X-ray spectroscopy (EDX), XRD analysis, and superconducting quantum interference device (SQUID) magnetometry (Figs. 4a, S6 and S7). Additionally, a quantitative analysis by inductively coupled plasma mass spectrometer (ICP-MS) showed that GON-3 was composed of 23.1 wt% Fe_3O_4 and 22.1 wt% Pd NPs. The formation of densely but uniformly distributed TOABr-Pd NPs enabled GON-3 to be highly dispersed in nonpolar media. A high loading amount of superparamagnetic Fe_3O_4 NPs within GON-3 induced fast separation of GON-3 from the reaction medium using an external magnet (Fig. 4b and c). These results are in striking contrast to the traditional electrostatic assembly-induced GONs that exhibit a relatively slow magnetic response and low saturated magnetization value (Figs. 4d and S8). Furthermore, the fast magnetic separation of the catalyst can enhance its recycling stability and efficiency.

Based on these results, we investigated the catalytic activity and feasibility of GON-3 in Suzuki–Miyaura cross-coupling reaction between organic boron compounds and organic halides in nonpolar media. Eight different aryl halides were reacted with phenylboronic acid in the presence of TBAB in toluene at 110 °C for 24 h as shown in Table 1. Botella et al. reported that TBAB could enhance the coupling reaction rate by the formation of a boronate complex [45]. When GON-3 was added to the reaction

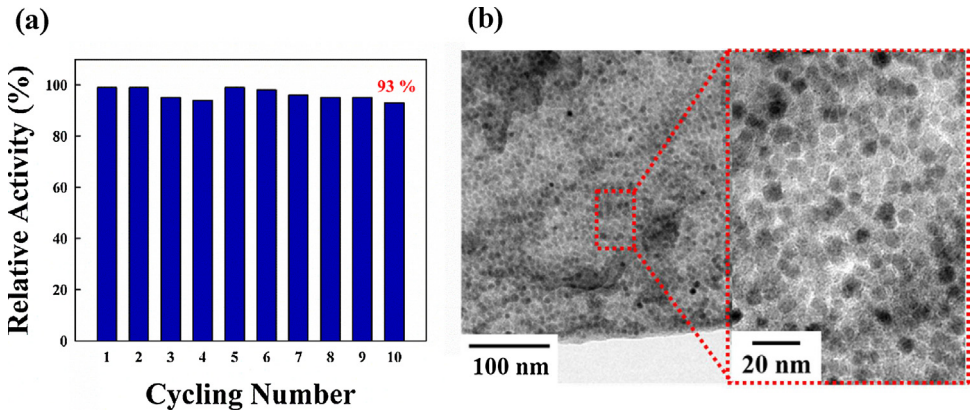

Fig. 5. (a) Recycling stability of the GON-3 catalyst in a Suzuki–Miyaura reaction. (b) TEM images of GON-3 after a Suzuki–Miyaura reaction.

Table 1
Suzuki–Miyaura cross-coupling reaction of aryl iodide and phenylboronic acid using the hydrophobic GON-3 catalyst in toluene.

Entry[a]	Aryl halide	Solvent[b]	Product	Yield (%)[c]
1	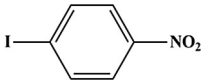	Toluene	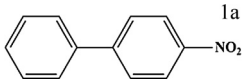 1a	99
2	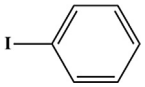	Toluene	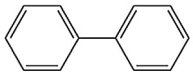 1b	99
3	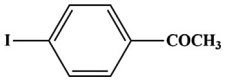	Toluene	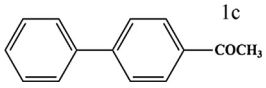 1c	88
4	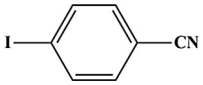	Toluene	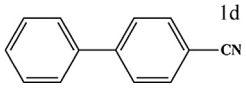 1d	70
5		Toluene	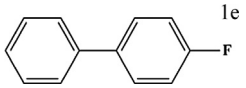 1e	66
6	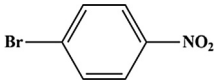	Toluene	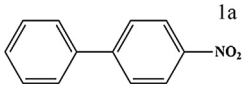 1a	85
7	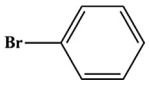	Toluene	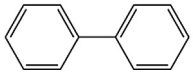 1b	99
8	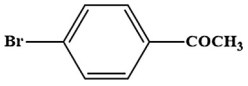	Toluene	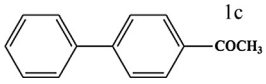 1c	78

[a] Reaction conditions: Ar-X (1 mmol), phenylboronic acid (2 mmol), tetrabutylammonium bromide (TBAB) (2 mmol), Na_2CO_3 (4 mmol) and toluene (3 mL) at boiling temperature under argon gas for 24 h.
[b] Represents the nonpolar solvent, catalyst: GON-3 (*i.e.*, GON/PEI/OA-Fe_3O_4 NP/PEI/TOABr-Pd NP) (Pd amount: 0.6 mol%).
[c] Isolated yield and products were determined by ^{1}H NMR and ^{13}C NMR spectroscopy. (NMR spectra for products 1a–1e are seen in the Supplementary data).

mixture, the product yields based on the reactant components were in the range 66–99% (Table 1), outperforming the yield achieved using metal ion reduction-induced GON catalysts in toluene (Entry 2 in Table 2). This high product yield using GON-3 was further confirmed by the comparison with previous reports (Table S1). When the outermost ligand of GON-3 was changed from TOABr to hydrophilic PEI, the resulting GON-3-PEI also exhibited high catalytic activity (99% yield) in aqueous and/or alcohol solvent (Table S2). However, hydrophilic GON-3-PEI exhibited low catalytic activity (18% yield) for the Suzuki–Miyaura reaction in toluene because of their aggregation (see Entry 1 in Table S2). These results imply that the catalytic performance of GON catalysts shown in our system strongly depends on the hydrophobicity and hydrophilicity of outermost ligands (or the dispersion stability of GON catalysts).

Although MWCNTs have also been widely used as solid supports for catalystic NPs, the specific surface area of GONs is larger than those of MWCNTs (220 $m^2 g^{-1}$) [46]. Therefore, the catalytic activity of GON-3 is reasonably predicted to exceed those of MWCNT catalysts under the same experimental conditions. To quantitatively confirm this assertion, the (PEI/OA-Fe_3O_4 NP/PEI/TOABr-Pd NP) multilayers were sequentially deposited onto carboxylic acid-functionalized MWCNTs (*i.e.*, MWCNT-1) (Fig. S9), and the catalytic activity in Suzuki–Miayaura reactions was then evaluated using the same total mass as previously used for the GON-3 catalyst (see Entry

Table 2
Suzuki–Miyaura cross-coupling reaction of aryl iodide and phenylboronic acid using GON-3, Metal ion reduction-induced GON and MWCNT-1 catalysts in toluene.

Entry[a]	Aryl halide	Catalyst[b]	Product	Yield (%)[c]
1	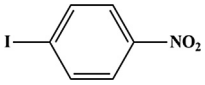	GON-3	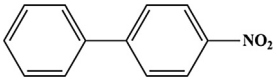	99
2	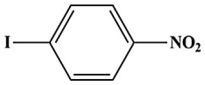	Metal ion reduction-induced GON	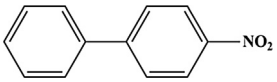	35
3	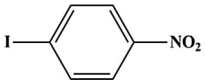	MWCNT-1	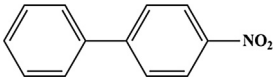	8

[a] Reaction conditions: Ar-X (1 mmol), phenylboronic acid (2 mmol), tetrabutylammonium bromide (TBAB) (2 mmol), Na_2CO_3 (4 mmol) and toluene (3 mL) at boiling temperature under argon gas for 24 h.
[b] Represents the catalyst: GON-3 (*i.e.*, GON/PEI/OA-Fe_3O_4 NP/PEI/TOABr-Pd NP), Metal ion reduction-induced GON (*i.e.*, GON/PEI/OA-Fe_3O_4 NP/PEI/Pd NP), MWCNT-1 (*i.e.*, MWCNT/PEI/OA-Fe_3O_4 NP/PEI/TOABr-Pd NP) (3 mg).
[c] Isolated yield and products were determined by ^{1}H NMR and ^{13}C NMR spectroscopy. (NMR spectra for products is seen in the Supplementary data).

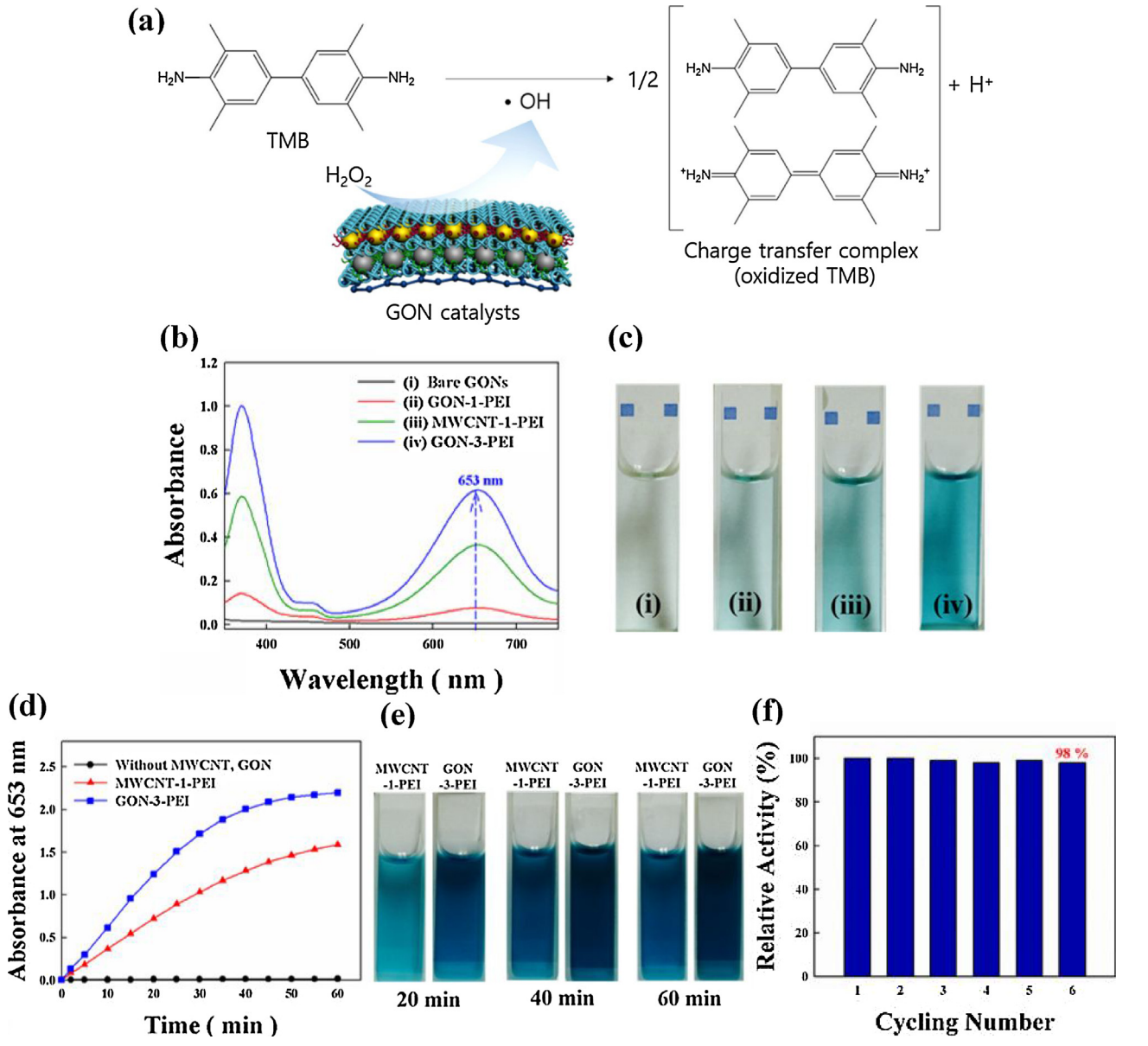

Fig. 6. (a) Schematic for oxidation of TMB catalyzed by GON catalysts. (b) UV–vis spectra of aqueous solutions after TMB oxidation by bare GONs, GON-1-PEI, MWCNT-1-PEI, and GON-3-PEI. The TMB oxidations were performed at 40 °C for 10 min. (c) Photographic images of the TMB oxidation solutions characterized in (b). (d) Time-dependent absorbance changes (at 653 nm) of the TMB oxidation solutions catalyzed by MWCNT-1-PEI and GON-3-PEI. (e) Photographic images of aqueous solutions containing MWCNT-1-PEI and GON-3-PEI with increasing reaction time from 20 to 60 min. (f) Recycling catalytic stability of GON-3-PEI.

3 in Table 2). In this case, the product yield obtained from GON-3 (including 22.1 wt% Pd NPs) was approximately 12 times higher than that from MWCNT-1 (including 4.56 wt% Pd NPs), which was primarily caused by a large amount of Pd NPs being adsorbed onto 2D-GONs.

We also investigated the extent of leaching of the Pd NPs following the Suzuki–Miyaura reaction in toluene by ICP–MS analysis. After the 10th reaction run, the amount of leached Pd was measured to be 0.85 ppm. This extremely low leaching amount of the Pd NPs is attributed to the formation of stable covalent bonds between the Pd NPs and PEI [47] as well as the strong magnetic response of GON-3 that prevent the partial loss of catalyst in the recovery process. As a result, GON-3 maintained a high catalytic activity of 93% even in 10th recycling tests, thereby demonstrating the stability of Pd and Fe_3O_4 NPs coating on the GONs (Fig. 5). Although the high loading of Pd NPs on the GONs could result in aggregation at high reaction temperature, the aggregation of NPs was not observed in the reaction system performed at 110 °C.

In addition to their ability to catalyze C—C coupling reactions, Pd NPs possess the peroxidaze-like ability to catalyze the H_2O_2-mediated oxidation of organic substrates such as TMB to decrease their toxicity and/or activate a color change, and thus can be used in the treatment of waste water or as a detection tool [48–50]. The TMB oxidation pathway by GON catalysts is shown in Fig. 6a. That is, the hydroxyl radicals (OH) formed by Pd NP-supported GON catalysts are reacted with TMB, producing the charge transfer complex (oxidized TMB). To further demonstrate the superior performance and versatility of the GON catalysts prepared from a ligand-replacement reaction in organic media, the oxidation of TMB by GON-3-PEI was investigated in aqueous media. Fig. 6b displayed the UV–vis spectra of four different buffer solutions of the bare GONs, GON-1-PEI, MWCNT-1-PEI, and GON-3-PEI containing 0.1 M NaOAc, 0.3 mM TMB, and 100 mM H_2O_2 at pH 4.0 [51,52]. The concentrations of the bare GONs and MWCNTs in the four different solution samples were adjusted to 0.5 wt%. The deposition of the outermost PEI ligand onto the hydrophobic Pd NP-coated GONs or MWCNTs enabled the resulting nanocomposites to be well dispersed in aqueous media as already mentioned. In this case, the bare GON solutions without TOABr-Pd and/or OA-Fe_3O_4 NPs exhibited no absorbance peaks in the measured wavelength range. In contrast, when the GON-3-PEI and MWCNT-1-PEI were added to the TMB solution with H_2O_2, the UV–vis spectra of the solutions displayed evident absorbance peaks (at 370 and 653 nm) corresponding to a visible blue color, implying the formation of the oxidized TMB. The intensity of the absorbance peak at 653 nm in the spectrum of the GON-3-PEI solution remarkably enhanced compared to that of the corresponding peak in the spectrum of the MWCNT-1-PEI solution, indicating that GON-3-PEI possessed more catalytic sites (as a result of its larger specific surface area) than MWCNT-1-PEI. These phenomena were easily detected by the naked eyes (Fig. 6c). Because the absorption bands from TMB oxidation are attributed to the charge-transfer complexes that originate from the one-electron oxidation of TMB and that correspond to a blue color with the characteristic absorbance peaks at 370 and 653 nm [49,51], these results demonstrate that the Pd NP-supported MWCNT and GONs decompose H_2O_2 into hydroxyl radicals (OH) that then oxidize the TMB substrate [50].

The GON-1-PEI catalyst without TOABr-Pd NPs also induced TMB oxidation (Fig. 6b). Recently, Fe_3O_4 NPs were reported to possess intrinsic peroxidase-like activity due to the presence of Fe^{2+} ions within OA-Fe_3O_4 NPs; this activity enabled GON-1-PEI to catalyze the oxidation of TMB in the presence of H_2O_2, generating a blue color [51–53]. However, given that the intensity of the absorbance peak at 653 nm was significantly lower (one-tenth) for GON-1-PEI than for GON-3-PEI, our results clearly indicate that GON-3-PEI accelerates the catalytic oxidation of TMB with an aid of TOABr-Pd NPs. Additionally, the oxidation of TMB by GON-3-PEI continued for approximately 60 min, as evidenced by a continuous change in the color of the TMB solution from light to dark blue, after which the reaction reached a plateau (Fig. 6d and e).

Furthermore, the recycling stability of GON-3-PEI was examined during repeated catalytic reactions (Fig. 6f). Similar to the recycling process in the Suzuki–Miyaura reaction, GON-3-PEI was magnetically separated from the reaction medium after the first TMB oxidation, washed with DI water, and redispersed for reuse. In this case, the catalytic activity in the 6th reaction and the leaching amount of Pd NPs after the 6th reaction exhibited 98% of the initial catalytic activity and were measured to be ~0.618 ppm, respectively. This high performance (*i.e.,* high catalytic activity and low level of leaching during recycling) of the hydrophobic/hydrophilic GON catalyst was entirely caused by the high loading amount and the stable immobilization of Pd and Fe_3O_4 NPs *via* covalent coordination to GONs, and furthermore by the facile control of the outermost ligand to establish hydrophobic and hydrophilic properties.

4. Conclusions

The GON catalysts prepared by consecutive ligand-replacement reaction exhibited remarkable catalytic performance and good recycling stability, allowing hydrophobic and hydrophilic dispersion in nonpolar and aqueous media, respectively. The high product yield obtained from the GON catalysts in Suzuki–Miyaura reaction in toluene outperformed previous results in the same solvent. When the outermost ligands on the GON catalysts were changed from hydrophobic TOABr to hydrophilic PEI, they also exhibited high catalytic activity in Suzuki–Miyaura reactions and TMB oxidation performed in hydrophilic media including water and alcohol. These results were primarily attributed to the facile control of the hydrophobicity and hydrophilicity of the outermost ligands as well as the densely packed catalytic NP arrays deposited onto the GONs. Furthermore, we believe that our ligand control approach can provide an important basis for resolving critical weaknesses of 2D-nanosheet catalysts, and designing high-performance catalysts with high activities and recycling stability for use in various reaction media.

Acknowledgements

This work was supported by the National Research Foundation (NRF) grant funded by the Ministry of Science, ICT & Future Planning (MSIP) (NRF-2015R1A2A1A01004354) and the Basic Science Research Program funded by the Ministry of Education (NRF-2017R1A6A3A04003192).

Appendix A. Supplementary data

Supplementary material related to this article can be found, in the online version, at doi: https://doi.org/10.1016/j.apsusc.2017.12.037

References

[1] L.D. Rampino, F.F. Nord, Preparation of palladium and platinum synthetic high polymer catalysts and the relationship between particle size and rate of hydrogenation, J. Am. Chem. Soc. 63 (1941) 2745–2749.
[2] L.N. Lewis, Chemical catalysis by colloids and clusters, Chem. Rev. 93 (1993) 2693–2730.
[3] A.T. Bell, The impact of nanoscience on heterogeneous catalysis, Science 299 (2003) 1688–1691.
[4] F. Zaera, Nanostructured materials for applications in heterogeneous catalysis, Chem. Soc. Rev. 42 (2013) 2746–2762.

[5] W. Long, N.A. Brunelli, S.A. Didas, E.W. Ping, C.W. Jones, Aminopolymer–silica composite-supported Pd catalysts for selective hydrogenation of alkynes, ACS Catal. 3 (2013) 1700–1708.
[6] R. Su, R. Tiruvalam, A.J. Logsdail, Q. He, C.A. Downing, M.T. Jensen, S. Wendt, C.R.A. Catlow, C.J. Kiely, G.J. Hutchings, F. Besenbacher, Designer titania-supported Au–Pd nanoparticles for efficient photocatalytic hydrogen production, ACS Nano 8 (2014) 3490–3497.
[7] N. Miyaura, A. Suzuki, Palladium-catalyzed cross-coupling reactions of organoboron compounds, Chem. Rev. 95 (1995) 2457–2483.
[8] R.F. Heck, Acylation, methylation, and carboxyalkylation of olefins by Group VIII metal derivatives, J. Am. Chem. Soc. 90 (1968) 5518–5526.
[9] K. Sonogashira, Y. Tohda, N. Hagihara, A convenient synthesis of acetylenes: catalytic substitutions of acetylenic hydrogen with bromoalkenes, iodoarenes and bromopyridines, Tetrahedron Lett. 16 (1975) 4467–4470.
[10] A. Balanta, C. Godard, C. Claver, Pd nanoparticles for C–C coupling reactions, Chem. Soc. Rev. 40 (2011) 4973–4985.
[11] P. Raveendran, J. Fu, S.L. Wallen, Completely "green" synthesis and stabilization of metal nanoparticles, J. Am. Chem. Soc. 125 (2003) 13940–13941.
[12] Y. Min, M. Akbulut, K. Kristiansen, Y. Golan, J. Israelachvili, The role of interparticle and external forces in nanoparticle assembly, Nat. Mater. 7 (2008) 527–538.
[13] G.M. Scheuermann, L. Rumi, P. Steurer, W. Bannwarth, R. Mülhaupt, Palladium nanoparticles on graphite oxide and its functionalized graphene derivatives as highly active catalysts for the Suzuki–Miyaura coupling reaction, J. Am. Chem. Soc. 131 (2009) 8262–8270.
[14] L. Duan, R. Fu, Z. Xiao, Q. Zhao, J.-Q. Wang, S. Chen, Y. Wan, Activation of aryl chlorides in water under phase-transfer agent-free and ligand-free Suzuki coupling by heterogeneous palladium supported on hybrid mesoporous carbon, ACS Catal. 5 (2014) 575–586.
[15] L. Li, H. Zhao, J. Wang, R. Wang, Facile fabrication of ultrafine palladium nanoparticles with size-and location-control in click-based porous organic polymers, ACS Nano 8 (2014) 5352–5364.
[16] J. Wang, S.A. Kondrat, Y. Wang, G.L. Brett, C. Giles, J.K. Bartley, L. Lu, Q. Liu, C.J. Kiely, G.J. Hutchings, Au–Pd nanoparticles dispersed on composite titania/graphene oxide-supports as a highly active oxidation catalyst, ACS Catal. 5 (2015) 3575–3587.
[17] T. Borkowski, J. Dobosz, W. Tylus, A.M. Trzeciak, Palladium supported on Al_2O_3–CeO_2 modified with ionic liquids as a highly active catalyst of the Suzuki–Miyaura cross-coupling, J. Catal. 319 (2014) 87–94.
[18] G.-Q. Kong, S. Ou, C. Zou, C.-D. Wu, Assembly and post-modification of a metal–organic nanotube for highly efficient catalysis, J. Am. Chem. Soc. 134 (2012) 19851–19857.
[19] D. Saha, R. Sen, T. Maity, S. Koner, Anchoring of palladium onto surface of porous metal–organic framework through post-synthesis modification and studies on Suzuki and Stille coupling reactions under heterogeneous condition, Langmuir 29 (2013) 3140–3151.
[20] S. Moussa, A.R. Siamaki, B.F. Gupton, M.S. El-Shall, Pd-partially reduced graphene oxide catalysts (Pd/PRGO): laser synthesis of Pd nanoparticles supported on PRGO nanosheets for carbon–carbon cross coupling reactions, ACS Catal. 2 (2011) 145–154.
[21] S. Santra, P.K. Hota, R. Bhattacharyya, P. Bera, P. Ghosh, S.K. Mandal, Palladium nanoparticles on graphite oxide: a recyclable catalyst for the synthesis of biaryl cores, ACS Catal. 3 (2013) 2776–2789.
[22] F. Giacalone, V. Campisciano, C. Calabrese, V.L. Parola, Z. Syrgiannis, M. Prato, M. Gruttadauria, Single-walled carbon nanotube–polyamidoamine dendrimer hybrids for heterogeneous catalysis, ACS Nano 10 (2016) 4627–4636.
[23] D. Chen, H. Feng, J. Li, Graphene oxide: preparation, functionalization, and electrochemical applications, Chem. Rev. 112 (2012) 6027–6053.
[24] S. Horikoshi, A. Osawa, M. Abe, N. Serpone, On the generation of hot-spots by microwave electric and magnetic fields and their impact on a microwave-assisted heterogeneous reaction in the presence of metallic Pd nanoparticles on an activated carbon support, J. Phys. Chem. C 115 (2011) 23030–23035.
[25] D.S. Su, G. Wen, S. Wu, F. Peng, R. Schlögl, Carbocatalysis in liquid-phase reactions, Angew. Chem. Int. Ed. 56 (2017) 936–964.
[26] J. Hu, Y. Wang, M. Han, Y. Zhou, X. Jiang, P. Sun, A facile preparation of palladium nanoparticles supported on magnetite/s-graphene and their catalytic application in Suzuki–Miyaura reaction, Catal. Sci. Technol. 2 (2012) 2332–2340.
[27] H.A. Elazab, A.R. Siamaki, S. Moussa, B.F. Gupton, M.S. El-Shall, Highly efficient and magnetically recyclable graphene-supported Pd/Fe_3O_4 nanoparticle catalysts for Suzuki and Heck cross-coupling reactions, Appl. Catal. A 491 (2015) 58–69.
[28] M. Sarvestani, R. Azadi, Palladium-nanoparticles deposited on a graphene–benzimidazole support as an efficient and recyclable catalyst for aqueous-phase Suzuki–Miyaura coupling reaction, Appl. Organometal. Chem. 31 (2016) 1–7.
[29] M. Gómez-Martínez, E. Buxaderas, I.M. Pastor, D.A. Alonso, Palladium nanoparticles supported on graphene and reduced graphene oxide as efficient recyclable catalyst for the Suzuki–Miyaura reaction of potassium aryltrifluoroborates, J. Mol. Catal. A: Chem. 404 (2015) 1–7.
[30] S. Stankovich, D.A. Dikin, G.H.B. Dommett, K.M. Kohlhaas, E.J. Zimney, E.A. Stach, R.D. Piner, S.T. Nguyen, R.S. Ruoff, Graphene-based composite materials, Nature 442 (2006) 282–286.
[31] Y. Xu, Z. Liu, X. Zhang, Y. Wang, J. Tian, Y. Huang, Y. Ma, X. Zhang, Y. Chen, A graphene hybrid material covalently functionalized with porphyrin: synthesis and optical limiting property, Adv. Mater. 21 (2009) 1275–1279.
[32] D.I. Gittins, F. Caruso, Spontaneous phase transfer of nanoparticulate metals from organic to aqueous media, Angew. Chem. Int. Ed. 40 (2001) 3001–3004.
[33] J. Puig, C.E. Hoppe, L.A. Fasce, C.J. Pérez, Y. Piñeiro-Redondo, M. Bañobre-López, J. Riavas, R.J.J. Williams, Superparamagnetic nanocomposites based on the dispersion of oleic acid-stabilized magnetite nanoparticles in a diglycidylether of bisphenol A-based epoxy matrix: magnetic hyperthermia and shape memory, J. Phys. Chem. C 116 (2012) 13421–13428.
[34] W.S. Hummers, R.E. Offeman, Preparation of graphitic oxide, J. Am. Chem. Soc. 80 (1958) 1339.
[35] T. Ramanathan, F.T. Fisher, R.S. Ruoff, L.C. Brinson, Amino-functionalized carbon nanotubes for binding to polymers and biological systems, Chem. Mater. 17 (2005) 1290–1295.
[36] S. Sun, H. Zeng, Size-controlled synthesis of magnetite nanoparticles, J. Am. Chem. Soc. 124 (2002) 8204–8205.
[37] L. Etgar, E. Lifshitz, R. Tannenbaum, Hierarchical conjugate structure of γ-Fe_2O_3 nanoparticles and PbSe quantum dots for biological applications, J. Phys. Chem. C 111 (2007) 6238–6244.
[38] D. Pan, N. Zhao, Q. Wang, S. Jiang, X. Ji, L. An, Facile synthesis and characterization of luminescent TiO_2 nanocrystals, Adv. Mater. 17 (2005) 1991–1995.
[39] X.Z. Lin, X. Teng, H. Yang, Direct synthesis of narrowly dispersed silver nanoparticles using a single-source precursor, Langmuir 19 (2003) 10081–10085.
[40] C. Wang, H. Daimon, T. Onodera, T. Koda, S. Sun, A general approach to the size-and shape-controlled synthesis of platinum nanoparticles and their catalytic reduction of oxygen, Angew. Chem. Int. Ed. 47 (2008) 3588–3591.
[41] J. Yang, C. Tian, L. Wang, H. Fu, An effective strategy for small-sized and highly-dispersed palladium nanoparticles supported on graphene with excellent performance for formic acid oxidation, J. Mater. Chem. 21 (2011) 3384–3390.
[42] J. Kim, L.J. Cote, F. Kim, W. Yuan, K.R. Shull, J. Huang, Graphene oxide sheets at interfaces, J. Am. Chem. Soc. 132 (2010) 8180–8186.
[43] X.-L. Li, Q. Peng, J.-X. Yi, X. Wang, Y. Li, Near monodisperse TiO_2 nanoparticles and nanorods, Chem. Eur. J. 12 (2006) 2383–2391.
[44] L. Pan, X.-D. Zhu, X.-M. Xie, Y.-T. Liu, Delicate ternary heterostructures achieved by hierarchical co-assembly of Ag and $Fe3O_4$ nanoparticles on MoS_2 nanosheets: morphological and compositional synergy in reversible lithium storage, J. Mater. Chem. A 3 (2015) 2726–2733.
[45] L. Botella, C. Nájera, A convenient oxime-carbapalladacycle-catalyzed Suzuki cross-coupling of aryl chlorides in water, Angew. Chem. Int. Ed. 41 (2002) 179–181.
[46] S. Shiraishi, M. Kibe, T. Yokoyama, H. Kurihara, N. Patel, A. Oya, Y. Daburagi, Y. Hishiyama, Electric double layer capacitance of multi-walled carbon nanotubes and B-doping effect, Appl. Phys. A 82 (2006) 585–591.
[47] J. Liu, X. Huo, T. Li, Z. Yang, P. Xi, Z. Wang, B. Wang, Palladium nanoparticles bonded to two-dimensional iron oxide graphene nanosheets: a synergistic and highly reusable catalyst for the tsuji–trost reaction in water and air, Chem. Eur. J. 20 (2014) 11549–11555.
[48] L. Su, J. Feng, X. Zhou, C. Ren, H. Li, X. Chen, Colorimetric detection of urine glucose based $ZnFe_2O_4$ magnetic nanoparticles, Anal. Chem. 84 (2012) 5753–5758.
[49] H. Wang, S. Li, Y. Si, Z. Sun, S. Li, Y. Lin, Recyclable enzyme mimic of cubic Fe_3O_4 nanoparticles loaded on graphene oxide-dispersed carbon nanotubes with enhanced peroxidase-like catalysis and electrocatalysis, J. Mater. Chem. B 2 (2014) 4442–4448.
[50] Y. Liu, D.L. Purich, C. Wu, Y. Wu, T. Chen, C. Cui, L. Zhang, S. Cansiz, W. Hou, Y. Wang, S. Yang, W. Tan, Ionic functionalization of hydrophobic colloidal nanoparticles to form ionic nanoparticles with enzymelike properties, J. Am. Chem. Soc. 137 (2015) 14952–14958.
[51] R. Long, H. Huang, Y. Li, L. Song, Y. Xiong, Palladium-based nanomaterials: a platform to produce reactive oxygen species for catalyzing oxidation reactions, Adv. Mater. 27 (2015) 7025–7042.
[52] X. Zheng, Q. Zhu, H. Song, X. Zhao, T. Yi, H. Chen, X. Chen, In situ synthesis of self-assembled three-dimensional graphene–magnetic palladium nanohybrids with dual-enzyme activity through one-pot strategy and its application in glucose probe, ACS Appl. Mater. Interfaces 7 (2015) 3480–3491.
[53] L. Gao, J. Zhuang, L. Nie, J. Zhang, Y. Zhang, N. Gu, T. Wang, J. Feng, D. Yang, S. Perret, X. Yan, Intrinsic peroxidase-like activity of ferromagnetic nanoparticles, Nat. Nanotechnol. 2 (2007) 577–583.